ELSEVIER

Contents lists available at ScienceDirect

Earth and Planetary Science Letters

www.elsevier.com/locate/epsl



An abrupt Middle-Miocene increase in fluid flow into the Leeward Margin Great Bahama Bank, constraints from δ^{44} Ca and Δ_{47} values



Philip T. Staudigel ^{a,*}, John A. Higgins ^b, Peter K. Swart ^c

- ^a Cardiff University, Main Building, Park Place, CF10 3AT, Cardiff, Wales, United Kingdom
- ^b Princeton University: Princeton, NJ, USA
- ^c University of Miami, Rosenstiel School for Marine and Atmospheric Science, Key Biscayne, FL, USA

ARTICLE INFO

Article history: Received 8 May 2020 Received in revised form 5 September 2020 Accepted 4 October 2020 Available online xxxx Editor: L. Derry

Keywords: carbonate diagenesis sedimentology calcium isotopes clumped isotopes fluid advection paleohydrology

ABSTRACT

The advection of seawater into the sediments deposited on the margins of Great Bahama Bank has been demonstrated to play in important role in ventilating the uppermost sediments, as well as supplying elements for diagenetic reactions deeper within the platform. Here, we implement a numerical model to calculate the rate of fluid advection at ODP Site 1003, using calcium isotopes as a tracer for fluid advection. A key parameter for this model, the rate of recrystallization of sediments, was constrained using the clumped isotope proxy. The model was tuned to existing datasets of clumped and carbonate calcium isotope measurements for this site. Results of this modeling effort indicate that, prior to \sim 15 Ma, fluids were advected into the platform at a rate substantially lower than the present day. The rate of advection abruptly increased \sim 13 Ma to a value greater than the present day. The increase in advective flux during the mid-Miocene coincides with a major reorganization of the platform from a ramp-like geometry to a steeper carbonate platform, indicating a change in the relative contributions of different mechanisms governing fluid flow on the platform margin and interior. This paper aims to explore the utility of using clumped and calcium isotopes to quantitatively reconstruct past fluid advection rates using this novel technique.

© 2020 Published by Elsevier B.V.

1. Introduction

The Great Bahama Bank (GBB) constitutes one of the few modern isolated carbonate platforms (Fig. 1A), making it a valuable natural laboratory for studying a depositional system that is extremely common in the depositional record (Schlager and Ginsburg, 1981). Ocean currents play an important role in governing the distribution of facies on the platform margin and channel (Lüdmann et al., 2016). In the present day, the prevailing benthic currents flow northward through the Santaren Channel and Florida Straits (Fig. 1a) and collectively account for 31.8 Sverdrup at 27°N with a mean surface velocity of 2.5 m/s, which decreases with depth (Wang and Mooers, 1998).

The larger-scale geometry of the platform margin is determined by the production of and redistribution of sediments. During the middle Miocene, tectonic uplift of the central American Seaway resulted in the uplift of the Isthmus of Panama, an event which resulted in an increase in the flow rate of ocean currents in the Straits of Florida (Haug and Tiedemann, 1998), which is evi-

E-mail address: staudigelp@cardiff.ac.uk (P.T. Staudigel).

denced by the appearance of large sediment drifts in the channel. This globally-synchronous disruption in ocean currents resulted in structural changes in the GBB and other carbonate systems at this time (Betzler and Eberli, 2019). Seismic cross sections (Fig. 1B) of the leeward margin of the GBB show that at approximately 12-12.5 Ma, the margin transitioned from a shallow-dipping carbonate ramp to a platform with a steeper margin (Betzler et al., 1999), associated with an increase in sediment production on the platform top "carbonate factory", and the onset of drift deposits, carbonate mounds and contourites in the channel (Anselmetti et al., 2000; Eberli et al., 2002; Lüdmann et al., 2016).

Numerous mechanisms exist which induce fluid circulation through carbonate platforms over timescales ranging over many orders of magnitude (Fig. 2). Surface and interior waves in the ocean can move fluids on timescales of seconds to minutes, tidal motion can flush fluids in a "twice daily" process (McCullough and Land, 1992a,b). Evaporation in platform interiors can result in the reflux of the resulting brine (Kaufman, 1994; Simms, 1984; Whitaker et al., 2004). Entrainment of fluid by regional water currents can force fluids through surface sediments (McCullough and Land, 1992a,b). Glacial-interglacial changes in sea level can result in a "eustatic pump" flushing a platform interior over 10 kyr-100 kyr timescales (Kaufman, 1994). Persistent

^{*} Corresponding author.

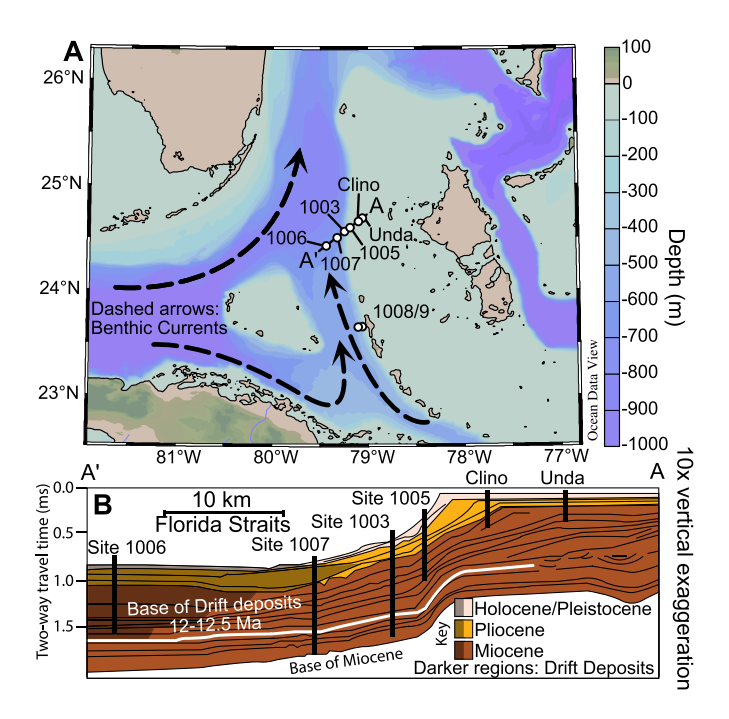


Fig. 1. Location figure. A) Orthographic projection map showing GEBCO 2019 15 arcsecond resolution gridded bathymetry data (gebco.net). Location of cores discussed in text and the "Western Line" seismic profile shown. Benthic currents described by Lüdmann et al. (2016) shown as dashed lines with arrows. Constructed using Ocean Data View, 2015 (odv.awi.de). B) "Western Line" seismic profile with location of Site 1003. Seismic line corresponding to base of drift deposits highlighted as a white line. Modified from Eberli et al. (2002).

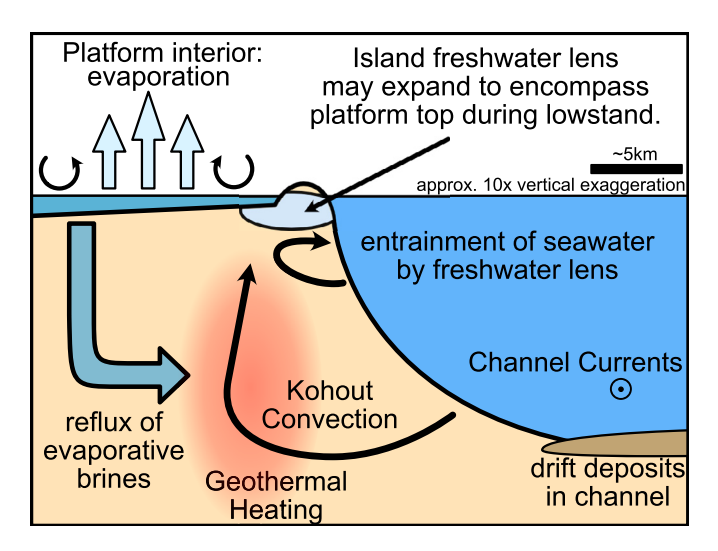


Fig. 2. Simplified diagram showing flow paths for different fluids through a carbonate platform margin and interior.

geothermally-driven advection (Kohout, 1965) can create circulation cells which extend beyond the distal edge of platform slope into the platform interior. Many forces can compete with one another on the platform at once; for example, the reflux of surface freshwater across the platform can affect the circulation driven by thermal processes (Whitaker et al., 2004). Reactive-transport modeling of carbonate margins shows that increases in evaporative brine production can restrict the geothermally-driven advection into the platform margin (Al-Helal et al., 2012).

Models of present-day fluid flow on the margin of the Great Bahama Bank indicate that the majority of the present advection into the platform is driven thermally (Caspard et al., 2004; Simms, 1984). This thermally-driven convection, termed Kohout-

convection (Kohout, 1965), is sensitive to the numerous factors relating to oceanography, changes in sediment type, and changes in platform architecture. Experimental modeling work conducted by Sanford et al. (1998) tested the influence of numerous variables on the fluid flow through a 2-D carbonate platform. In these models, the most significant factors governing advection rate are the intensity of the geothermal gradient and the permeability of the sediments, although the intensity can also be affected by changes in oceanographic conditions, as well as platform architecture. Evaporative brines can be transported laterally to more distal periplatform sediments (Fig. 2), the extent of this transport is itself a function surface processes, as well as the internal structure of the platform (Burchette and Wright, 1992). Interaction between the refluxed brines and Kohout convection cells can result in more complex situations wherein brines displace the advected seawater, effectively preventing the Kohout advection on platform margins into the platform interior (Whitaker et al., 2004). Therefore, changes in geometry, hydrology and sediment type during the evolution of a carbonate platform should be expected to be associated with changes in the location and intensity of fluid infiltration on the platform margins.

The advection of seawater constitutes an important flux of ions in the uppermost sediment, resulting in diagenetic reactions occurring in a more open system. If changes in advective flux can be correlated with larger-scale changes in platform architecture, then this would be of great interest to sedimentologists and geochemists seeking to understand the diagenetic history of the GBB, as well as many other ancient carbonate systems.

In this study, the changes in vertical fluid advection rates on the leeward margin of Great Bahama bank (ODP Leg 166, Site 1003) will be constrained, testing the hypothesis that the changes in platform margin geometry are correlated with changes in the intensity of fluid infiltration in the Bahamas. Although this theory will be tested in the Bahamas, similar predictions could be made regarding ancient sedimentary systems, specifically that changes in margin geometry would be expected to affect regional fluid flow, which in turn is expected to have a corresponding impact on the geochemistry of authigenic minerals forming in the sediments.

Sediment cores recovered by ODP Leg 166 were squeezed for pore fluids, analysis of these fluids revealed that the uppermost 40 m porefluid remained virtually unchanged (Kramer et al., 2000; Swart, 2000). These sediments also showed an absence of geothermal gradient in the same interval (Nagihara and Wang, 2000), indicating the presence of rapid flux of bottom seawater in this interval. A characteristic pattern is observed in the margin transect cores (Sites 1003 - 1007), wherein more platform proximal sediments featured larger flushed zones (maximum 60 mbsf at Site 1005) whereas the platform distal Site 1006 had a diminished flushed zone. Sites 1008 and 1009, which were recovered from a less steep portion of the platform margin had weaker flushed zones (Eberli et al., 1997; Chapter 11). Analyses of uranium concentrations and isotope ratios within the porefluids from the platform-proximal Site 1009 (Henderson et al., 1999) indicated a present-day advective fluid flow rate of 10.6±3.4 cm/yr. Similar flushed zones were noticed adjacent to other carbonate platforms and continental shelves (Betzler et al., 2017; Feary et al., 2000). This magnitude of advection of fluid results in volumes of water being flushed through the sediment column, resulting in a largely open-system diagenetic behavior; a system wherein the isotopic composition of sediments can be rapidly overprinted during the early neomorphism from aragonite to calcite (Ahm et al., 2018; Staudigel and Swart, 2019). Although the flushed zone is prominent in the present day sediments in the Bahamas and elsewhere. its intensity in the past remains largely unknown. Higher concentrations of strontium and more negative δ^{44} Ca values in the deeper

core (Higgins et al., 2018), suggesting far lower advection rates during the early Miocene.

The stable isotopes of calcium provide a useful tool for studying fluid advection. Primary carbonate sediments are isotopically lighter than seawater calcium (De La Rocha and DePaolo, 2000), the degree of fractionation is rate dependent (Lemarchand et al., 2004) such that the slower recrystallization during carbonate diagenesis tends to not measurably fractionate calcium isotopes (Fantle and DePaolo, 2007). The formation of authigenic carbonate, particularly in the uppermost sediments where seawater calcium can be supplied readily, can affect bulk δ^{44} Ca values (Ahm et al., 2018; Fantle and Ridgwell, 2020). This effect is pronounced in sediments with lower concentrations of carbonate, which has the potential to obscure, or even result in contradictory records of global climate events (Fantle and Ridgwell, 2020). The abundant carbonate sediment in the Bahamas would likely by robust to these authigenic effects, although there is evidence for bacterial sulphate reduction (BSR) accompanied with a corresponding increase in alkalinity centered around 200 mbsf (Kramer et al., 2000; Rennie and Turchyn, 2014). Despite this increase in alkalinity, there is less evidence for significant fractions of net precipitation of carbonate minerals, as there is no corresponding depletion in calcium ions at this depth (Kramer et al., 2000). It is possible however that the depletion of sulfate played a role in favoring the formation of replaceative dolomite at this depth (Baker and Kastner, 1981).

The influence of fluid advection on numerous shallow carbonate systems was assessed by Ahm et al. (2018), who constructed a model to describe the diagenetic behavior of ODP Site 1003, among other sites using variable water-rock ratios. The Ahm model did not attempt to consider the specific depositional history of these sites, and thus made no attempt to calculate the past magnitude of these advective fluxes. To this end, we have coupled a depositional model for ODP Site 1003 with a reaction-diffusion-advection model in order to determine changes in the intensity of fluid advection through the sediment column over time. The rate of recrystallization of these sediments is constrained using a published dataset of clumped isotope measurements for the same site (Staudigel and Swart, 2019).

2. Methods

2.1. Reaction-diffusion-advection model for ODP Site 1003

The calcium isotope ratio in carbonate and corresponding pore fluids is modeled using a reaction-diffusion-advection (RDA) model (Fig. 3). This model approximates the sedimentary column as a 1-dimensional system wherein seawater is advected at the top of the sediment column, and flows down at a constant velocity and is expelled from the bottom of the sediment column. The column is divided into a number of sub-units which communicate with the units above and below them through diffusion and advection. The uppermost unit communicates with a fixed-concentration boundary condition (seawater), and the lowermost unit exchanges with a lower non-diffusive (mirror) boundary condition.

In order to construct a model that accounts for sedimentation and compaction, while remaining computationally efficient, a marker-in-cell approach wherein the depth of the top of each unit is defined by a Lagrangian point (Gerya, 2010) was implemented. This point moves in space and time according to the surface sedimentation rate adjusted for the subsequent compaction. All parameters used to construct the model are described below and summarized in Table 1.

The degree of compaction downcore was estimated using porosity, as calculated by Staudigel and Swart (2019) from logging data from the initial reports from ODP Leg 166 (Eberli et al., 1997), where the porosity is calculated relative to depth.

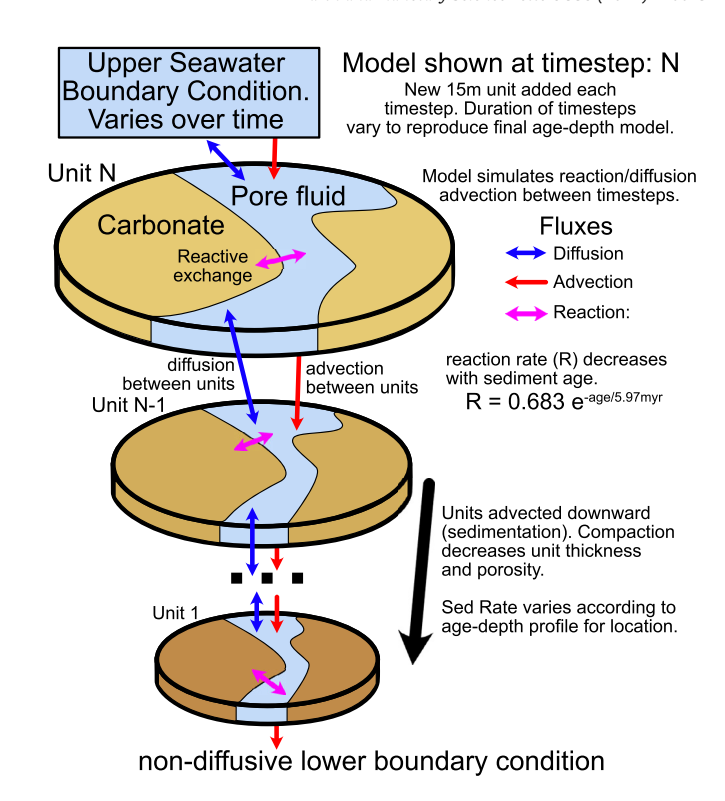


Fig. 3. Schematic of reaction-diffusion-advection (RDA) model used to simulate calcium isotope exchange during diagenesis.

$$(\phi) = 0.230 + (0.622 - 0.230)e^{-\text{depth}/470 \text{ m}}$$
 (1)

The instantaneous sedimentation rate for any instant in the model is calculated using the biostratigraphic age model (Wright and Kroon, 2000) adjusted for compaction, as shown in equation (2)

$$SR = SR_0 * (1 - \phi(0m)) / (1 - \phi(depth))$$
 (2)

Over each timestep of the model, a new sedimentary unit of a predefined thickness (15 m), is emplaced at the top of the sediment column. The RDA model simulates the chemical behavior of all sediment packages for the duration of time required to deposit another sediment unit of the same thickness. The burial depth of each unit is tracked within the differential equation and is adjusted within the model. New sedimentary units are comprised of 10 mol/kg calcium, whose primary 44 Ca/ 40 Ca ratio varies over time in unison with changes in seawater calcium isotope ratios.

The concentration of calcium in seawater has varied through time but and is calculated in this model using the relationship used by Zhang et al. (2020), where t is the time before present in Myr (Equation (3)).

$$mCa_{(t)} = 10.62 + 0.161t$$
 (3)

The modeled calcium isotope ratio of seawater changes linearly from -0.2% (relative to the present day ratio) at 23 Ma to 0% in the present day (Blättler et al., 2012; Farkaš et al., 2007), reaching at the modern $^{44}\text{Ca}/^{40}\text{Ca}$ ratio of 0.0221518 (Schmitt et al., 2001). New carbonate sediment forms at equilibrium with respect to the seawater isotope ratio with an alpha value of 0.9986, although this value can be changed in the model to account for different coefficients for calcite and aragonite if needed. This alpha-value is used as it is similar to values measured for uppermost sediments at Site 1003, as well as surface sediments from the Bahamas (Higgins et al., 2018).

Table 1Summary table for parameters used in the RDA model.

Parameter	Value or equation	Reference
Initial sediment depth	0 mbsf	n/a
Sedimentation rate	Variable: derived from age model	Wright and Kroon (2000)
Porosity (Site 1003)	$\phi = 0.230 + (0.622 - 0.230) e^{-depth/470 m}$	Eberli et al. (1997)
Temperature (Site 1003)	$T(^{\circ}C) = 10 + 33 \times depth(mbsf)$	Eberli et al. (1997)
Diffusivity of Ca	$D_{Ca}^0 = 3.60 \times 10^{-6} + 0.179 \times 10^6 T (^{\circ}C) (\text{cm}^2/\text{s})$	Boudreau (1997)
Diffusivity adjusted for sediment tortuosity	$D_{Ca} = \frac{D_{Ca}^0}{1 - \ln(\phi^2)} \text{ (cm}^2/\text{s)}$	Boudreau (1997)
Seawater [Ca ²⁺]	$[Ca_{sw}^{2+}] = 10.62 + 0.161 \times t \text{ (mM)}$	Zhang et al. (2020)
Seawater δ^{44} Ca	$\delta^{44} \text{Ca}_{\text{SW}} = \frac{-0.2\%_0}{23m\text{Vr}} \times t$	Blättler et al. (2012)
Modern seawater ⁴⁰ Ca/ ⁴⁴ Ca	45.153	Schmitt et al. (2001)
Sediment $\alpha_{\text{carb-water}}$	$R^{44}Ca_{sed} = 0.9986 * R^{44}Ca_{sw}$	Higgins et al. (2018)
Authigenic $\alpha_{carb-water}$	$R^{44}Ca_{authigenic} = 1.0000 * R^{44}Ca_{porefluid}$	Fantle and DePaolo (2007)
Sediment Age Rate	1 myr/myr	n/a
Initial sediment age	0 myr	n/a
Sediment reaction rate	$R = 0.693 * e^{-age/5.97myr}$	Staudigel and Swart (2019))
Sediment density	$ \rho_{\rm carb} = 2.7 \text{ g/cm}^3 $	n/a
Seawater density	$\rho_{\rm W} = 1.03 {\rm g/cm^3}$	n/a

The concentration of a given isotope in the fluid (C_f) , changes over time according to a one-dimensional reaction-transport equation given by equation (4)

$$\frac{\partial C_f}{\partial t} = D_C \frac{\partial^2 C_f}{\partial z^2} + v \frac{\partial C}{\partial z} + Rm \left(C_s - C_{eq} \right) \tag{4}$$

The concentration of the same isotope in the solid is governed purely by the reactive term, according to equation (5)

$$\frac{dC_s}{dt} = -R\left(C_s - C_{eq}\right) \tag{5}$$

The fractionation of calcium isotopes is modeled such that $\alpha = 1.000$ (Fantle and DePaolo, 2007). The mass ratio constant, m, is calculated using the porosity of each sedimentary unit, as well as using the densities of water ($\rho_{\rm w} = 1.03~{\rm g/cm^3}$) and calcium carbonate ($\rho_{\rm c} = 2.7~{\rm g/cm^3}$), following

$$m = \frac{\rho_c \left(1 - \phi\right)}{\rho_w \phi} \tag{6}$$

For calcium isotopes, the diffusion coefficient, D_c is calculated following the methods outlined in Boudreau (1997), the diffusivity of infinitely diluted calcium in water (here calculated in cm²/s) is related to temperature following

$$D_{\mathsf{Ca}}^{0} = 3.60 \times 10^{-6} 0.179 \times 10^{6} \mathsf{T} \tag{7}$$

Following the reasoning outlined by Fantle and DePaolo (2007) this diffusivity is used for all isotopes of calcium, as hydrated ions tend to diffuse at similar rates, irrespective of isotopic mass (Gussone et al., 2003). This diffusivity is adjusted for the tortuosity of the pore volume

$$D_{\mathsf{Ca}} = \frac{D_{\mathsf{Ca}}^0}{\theta^2} \tag{8}$$

where the tortuosity factor, θ^2 , is defined relative to porosity following the modified Maxwell-Weissburg relationship (Boudreau, 1997).

$$\theta^2 = 1 - \ln(\phi^2) \tag{9}$$

In our model, D_{Ca} ranges between 8500-11000 m^2/myr , reaching a minimum diffusivity at 200 mbsf.

The uppermost unit exchanges with a upper seawater boundary condition; exchange is simulated as if it were an overlying sediment package. The lower boundary condition is a simple zero-flux boundary condition with respect to diffusion. The differential

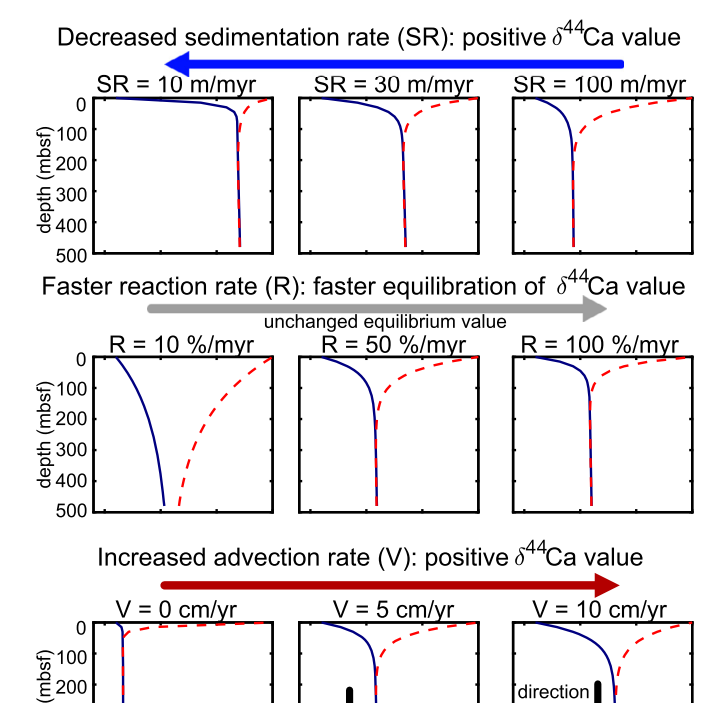


Fig. 4. Modeled pore fluid and carbonate downcore $\delta^{44}\text{Ca}$ values for simulations with variable Sedimentation Rate (SR: top row), Reaction rate (R: middle row) and advective Velocity (V: bottom row). Parameter values (unless otherwise specified) are $\delta^{44}\text{Ca}_{\text{Sed}}$: -1.4%, $\delta^{44}\text{Ca}_{\text{Sw}}=0\%$, SR = 60 m/myr R = 70%/myr V = 5 cm/yr. Default value set shown in bottom middle figure. All other parameters are the same as from Table 1. Blue solid line: Carbonate sediment $\delta^{44}\text{Ca}$ value; red dashed line: fluid $\delta^{44}\text{Ca}$ value. (For interpretation of the colors in the figure(s), the reader is referred to the web version of this article.)

-1.0

 δ^{44} Ca (‰ seawater)

-1.5

-0.5

flow

-1.0

 δ^{44} Ca (‰ seawater)

-1.5

equations associated with this model are integrated over each sedimentary timestep using Matlab's *ode15s*.

In order to evaluate the sensitivity of this model for recrystallizing calcium isotopes to variables such as sedimentation rate, recrystallization rate and advective flow magnitude, a series of model runs were conducted using different values for these parameters (Fig. 4). The range of parameters tested in Fig. 4 represent a range of plausible values expected for ODP Site 1003.

9 400 400

-0.5

-1.0

 δ^{44} Ca (‰ seawater)

The model simulates the advection and diffusion of solutes in a simplified 1-dimensional case, wherein fluid enters the sediment column and flows vertically through the entire stack. Although this approximation is relatively common in the literature (Fantle and DePaolo, 2007; Henderson et al., 1999; Richter and DePaolo, 1987; Zhang et al., 2020), this method may not fully capture the complex, three-dimensional fluid flow expected in platform margins and interiors (Caspard et al., 2004; Sanford et al., 1998; Simms, 1984; Whitaker et al., 2004). Therefore, this manuscript will limit itself to discussion of the results of this simplified vertical component which can be resolved using the available data. It is possible for future models to implement more nuanced hydrological models, which could account for fluid flowing in additional dimensions

2.2. Constraining recrystallization rate using clumped isotopes

Clumped isotopes record paleotemperatures and are generally unaffected by changes in fluid chemistry and thus are a useful tool for studying the chemical alteration of carbonate sediments (Staudigel et al., 2018a,b; Staudigel and Swart, 2019). In the Bahamas, surface sediments form at warm temperatures, then recrystallize at the cooler benthic temperatures; further recrystallization occurs during burial at elevated temperatures due to the geothermal gradient. In sediment recovered by ODP Site 1003, the more deeply buried sediments report warmer temperatures as well as more positive fluid δ^{18} O values when reconstructed using clumped isotopes; indicative of recrystallization at depth within a closed system (Staudigel and Swart, 2019). A model was presented in the previous study, which simulates the evolution of clumped isotope distributions during burial, wherein several possible models for recrystallization rate were presented, which are broadly described by the following equation modified from (Richter and DePaolo, 1987).

$$R_p = A + B \times e^{-age/C} \tag{10}$$

$$R_{D} = \beta \times R_{D} \tag{11}$$

In these equations, R_p refers to the rate of recrystallization of pristine material, and R_D refers to the rate for diagenetically altered material. Using the clumped isotope data, the values for the recrystallization parameters were determined using a gradient-descent technique, which was conducted using the *nlinfit* function in Matlab, using the "Statistics and Machine Learning" toolbox.

The full form of these equations requires four parameters to fit a given dataset, and optimization of these parameters yields ambiguous results wherein multiple values provide equally good fits resulting in no unambiguous minima for the fit, this was because greater A values and longer lapse rates (expressed as C in equations) fit the clumped isotope data equally well. To remedy this, the clumped isotope dataset has been fit here using a simplified version of this function wherein the first term, A is set to zero. When these model constants are optimized, the best-fit value for β is found to be 0.99 \pm 0.32, it was therefore assumed to be equal to 1 and the best-fit parameters were found for B and C. In order to evaluate the uncertainties associated with this estimate: the fitting algorithm was repeated using a bootstrap resampling of the original dataset (Fig. 5).

Using the recrystallization rate constants determined using this method, five iterations of the calcium isotope model were run using forced advective flow (Fig. 6).

2.3. Calculating advective flow rate over time

Using the recrystallization rate constants determined from the Δ_{47} proxy, the rate of vertical fluid advection can be calculated using a similar gradient-descent algorithm as was used in

the previous section but applied to the calcium isotope data using the RDM. In simplified terms: the optimization process runs the RDA model hundreds of times, each time refining advection rates at specified time points. When the output of the RDA best matches the $\delta^{44}\text{Ca}$ values of the carbonates, i.e. no better solutions can be arrived at with further optimization, then the algorithm is complete. This model is run multiple times on bootstrap re-weighted calcium isotope datasets for Site 1003 in order to determine the uncertainty caused by uncertainties in the measurements.

A user-specified number of points in time are defined, which span the age of sediments. The default distribution is such that these are evenly sampled with respect to depth, this means that there is a roughly even number of calcium isotope measurements between each point. The model reads these values and interpolates between them in order to calculate an instantaneous vertical fluid advection rate for a given time. This model can only compute the vertical component (i.e. parallel to the core itself) of the advective flux, thus the absolute rate of advection may be higher. The fitting algorithm first guesses that all time points had an advective flux of zero, it subsequently refines these values through progressive iteration of the model. The calcium isotope model takes approximately 2 minutes to complete on a personal computer with a spatial resolution of 15 m. The fitting algorithm requires several hundred iterations of this model, thus this fitting algorithm requires substantial time to complete on a personal computer, taking several hours to days depending on the number of changes in advective rate desired and the desired spatial resolution.

The fitting algorithm initially solves a coarse temporal resolution, using eight tie points and calculating a best-fit advective rate for each of these which then are interpolated into 16 points which are subsequently refined. This approach is taken in order to prevent the Gradient-descent algorithm from getting stuck in a sub-optimal solution. Attempts to resolve beyond this temporal resolution yield diminished returns and will tend to over-fit data.

In order to evaluate the uncertainties associated with the calculated vertical advection rates, the calcium isotope dataset was resampled multiple times using a bootstrapping method, the best-fit advection rates for each of these resampled datasets were then calculated. This allows for variance in the dataset to be considered when calculating the best-fit advection rates. This bootstrapresampled computation, which subsampled the dataset 200 times, was implemented using the ARCCA Cluster at Cardiff University taking three days to run on four nodes. Matlab scripts that are used to construct and refine these models are provided as a supplementary file.

It is important to note that this algorithm, as with the reaction-diffusion model, assumes the system to be 1-dimensional along axis of the sediment core in a complex, evolving, threedimensional sedimentary system. This problem was also encountered at Site 1009 by Henderson et al. (1999) while reconstructing modern advection rates. They overcame this issue by assuming that the flow was predominantly horizontal and multiplying their vertical results by $1/tan(\theta)$ (where θ is the angle of the surface relative to horizontal). Because the horizontal and vertical components may change over time, we cannot apply a simple trigonometric rescaling to our results. Increases in the horizontal motion of fluid are expected to be accompanied with corresponding increases in path length; in a horizontal system, the increase in path length from horizontal motion would thus increase the amount of carbonate available for exchange. In a perfectly horizontal system, which is equally hypothetical, then the increased path length and increased advective velocity terms would cancel out such that again the only relevant term is the vertical motion of the fluid. This assumption is not entirely true in our case, however, due to the variable slope angle over the core it is difficult to apply a consistent trigonometric correction to our data. Because the permeability of sediments to fluid flow can vary between the horizontal and vertical exes, it is possible that shifts in the direction of flow may result in changes in the flow rate; because this algorithm solves for fluid flow rate independently, this particular detail is not explored in greater detail in this manuscript. The application of a more complex hydrological model to our site could accommodate many such complexities, and allow for more direct calculation of the underpinning forces controlling fluid flow.

2.4. Calcium and Clumped Isotope Datasets for Site 1003

Existing datasets for carbonate clumped isotope (Staudigel and Swart, 2019; N=70) and carbonate calcium isotopes (Higgins et al., 2018; N=88) are used to determine the best-fit parameters for the models used in this study. Details regarding their acquisition are provided as a supplementary text to this manuscript.

3. Results

3.1. Calcium model sensitivity analysis

In order to test the sensitivity of the calcium isotope system to changes in burial conditions, the calcium isotope model was run using variable sedimentation rate, recrystallization rate, and advection rate (Fig. 4). Each model simulated the deposition of 500 meters of sediment with a box thickness of 15 m with a porosity of 60% (no compaction). Models show that slower sedimentation rates resulted in more positive equilibrium δ^{44} Ca values in these model runs (Fig. 4, top row). Increased reaction rate results a more rapid approach to equilibrium δ^{44} Ca values, however with no significant change in the equilibrium value itself (Fig. 4, middle row). Lastly, increased advection rate results in more positive equilibrium δ^{44} Ca values (Fig. 4, bottom row).

3.2. Best-fit reaction rate constants

The gradient descent algorithm was used to determine the best-fit recrystallization rates for carbonate at Site 1003. Bootstrap resampling of the clumped isotope dataset was used to examine the sensitivity of this regression, the results for 1000 permutations of the bootstrapped datasets are shown in Fig. 5. The best-fit values for calculating reaction rate over time (± 1 std.error of the mean), which will be used in later models, is described by the equation (12).

$$0.693(\pm 0.187)e^{-\text{age}/5.97(\pm 2.78)\text{myr}}$$
 (12)

The uncertainties between estimates of the initial rate of recrystallization and the lapse rate are correlated with one another, appearing to follow an inverse relationship (Fig. 5a). The best-fit model describes the available $T\Delta_{47}$ data with an r^2 value of 0.63 (N = 70, p \ll 0.001) (Fig. 5b). These results are within the range calculated by Higgins et al. (2018) for initial recrystallization rate (0.1–1.0 myr⁻¹), which were determined using calcium isotopes in porefluids at Site 1003.

These reaction rates were input into the calcium isotope model using the burial history for ODP Site 1003. This depositional model was forced with advection rates ranging between 0 and 10 cm/yr, the output of which is shown in Fig. 6. These model runs illustrate that much of the variance in calcium isotopes result from changes in sedimentation rate. Periods of diminished sedimentation (200 mbsf or 1200 mbsf) are accompanied with more positive calcium isotope ratios.

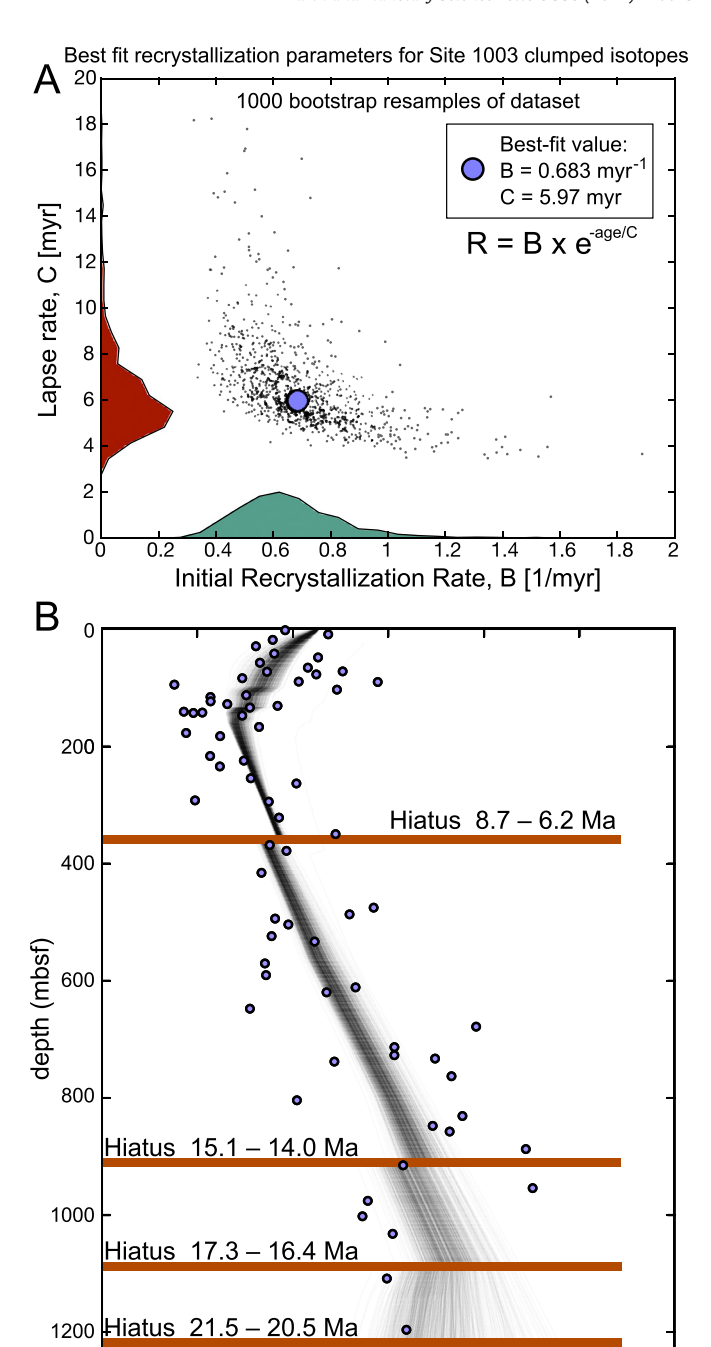


Fig. 5. Clumped isotope data for ODP Site 1003 fitted for reaction rate. A) Best-fit reaction rate coefficients for 1000 bootstrap resamples of $T\Delta_{47}$ data Staudigel and Swart (2019). B) Downcore measured (circles) and modeled (lines) $T\Delta_{47}$ values for ODP Site 1003 carbonate.

30

TΔ47 (°C)

40

50

60

20

There is local agreement between measured and modeled values, the model run with 2.5 cm/yr advection rates gives results similar to measured δ^{44} Ca values for sediments deposited below 900 mbsf, although it yields consistently too negative values for sediments above this depth. Models with advection of 5.0 cm/yr yield results more in agreement with the sediments above 900 mbsf. The model where V = 5 cm/yr was the best-fitting model, with a coefficient of determination of 0.33.

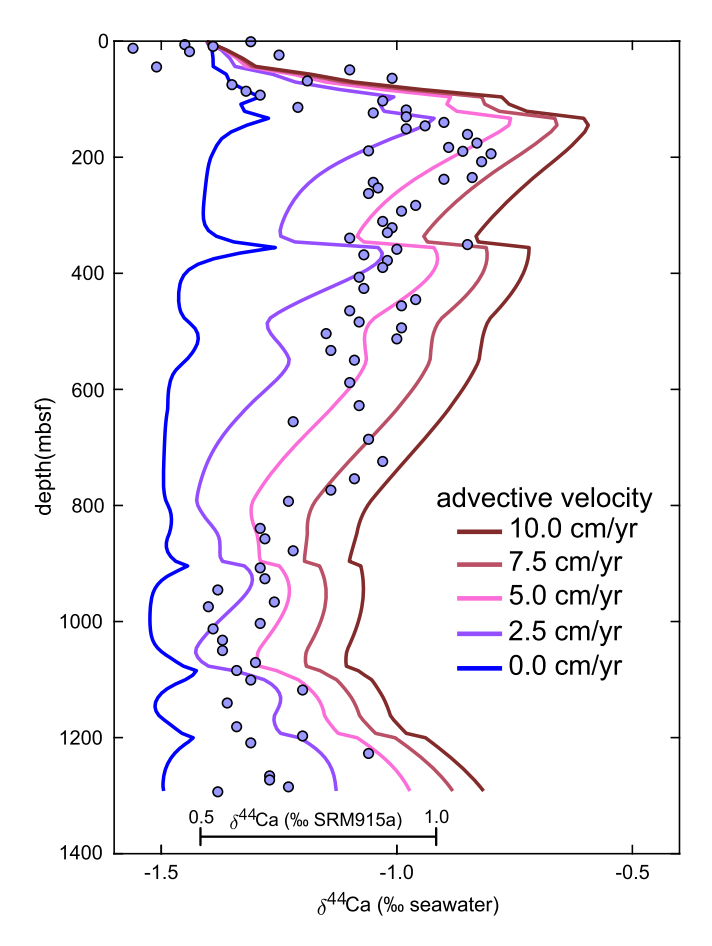


Fig. 6. Calcium isotope model using ODP Site 1003 depositional history and reaction constants determined using clumped isotopes. Model was implemented using advective velocities of 0.0 cm/yr – 10.0 cm/yr (solid lines). δ^{44} Ca values for ODP Site 1003 (blue dots) from Higgins et al. (2018) shown.

3.3. Best-fit advection rates

The best-fit advective flux models for the resampled δ^{44} Ca values (200 iterations) are shown in Fig. 7a. The median best-fit calcium isotope model (solid red line in Fig. 7) explained the measured variance in the complete dataset of δ^{44} Ca values from Higgins et al. (2018) with $\rm r^2$ value of 0.77.

The best-fit calcium isotope models indicate that median vertical advection rates between 23 and 15 Ma ranged between 0.0 and 5 cm/year, averaging <2 cm/yr before 13 Ma (Fig. 7a). At 13 Ma, calculated advection rates increase, reaching a peak advection rate of 21.7 cm/yr at 12 Ma. Between 12.5 and 4 Ma, two separate advection maxima at 12 and 4.5 Ma, are observed. These "Advective Pulses" were separated a period where advection decreased to as low as 1 cm/yr, the longest hiatus in deposition occurs between the two peaks and a significant horizon of mud caps this non-depositional surface. The earliest pulse (Labeled P1) reached a peak advective flux rate of 22 ± 14 cm/yr (95% confidence). The second advective pulse (Labeled P2) lasted between 6 Ma and 3 Ma with a broad peak in vertical advection rate of 8 ± 3 cm/yr, which decreased into the Pliocene.

The youngest sediments have the highest degree of uncertainty in their advective rates when calculated using our model (Fig. 7a). This is due to these sediments undergoing initial stages of recrystallization, thus the model approaches a singularity for pristine sediment irrespective of advection rate; therefore, the modeled δ^{44} Ca value is relatively insensitive to the advective rate for modern advection rate in the model. In the uppermost sediments, the porefluid δ^{44} Ca gradient was approximately 1%/100 m (Higgins

et al., 2018), this gradient can be used to estimate the most recent advection rates. The gradient can be accommodated with a present-day advection rate of \sim 5 cm/yr (Fig. 4), which agrees with the median value estimated from the carbonate model (Fig. 7a).

4. Discussion

The distribution of calcium isotopes in sedimentary carbonate rocks can be affected diagenetically through a number of factors, all of which relate to the supply of calcium to recrystallizing sediment (Fantle and DePaolo, 2007; Fantle and Ridgwell, 2020), several of these factors (sedimentation, recrystallization and advection rate) are tested as variables in Fig. 4. Due to the abundance of calcium in carbonate minerals, and the relative paucity of calcium in modern seawater, significant quantities of seawater are necessary in order to significantly affect the calcium isotope composition of limestone (Ahm et al., 2018), thus: calcium is considered to be one of the most rock-buffered elements in the CaCO₃-seawater system.

Clumped isotopes, which are a non-conservative property of the carbonate mineral, behave in an opposite manner to calcium isotopes, as they cannot be rock-buffered. Clumped isotopes therefore make an ideal tool for constraining the rate of recrystallization of sediments. In the case of the Bahamas, sediments recrystallize rapidly due to the neomorphism of metastable aragonite to the more stable calcite, at Site 1003 the initial rate of recrystallization is $0.693 \pm 0.0.308 \text{ myr}^{-1}$ ($\pm 95\%$ confidence) (Fig. 5a). This estimate for recrystallization rate from clumped isotopes largely agrees with estimates from pore-fluid calcium isotopes measured by Higgins et al. (2018), which indicated an initial rate of recrystallization between 1.0 and 0.1 myr⁻¹. This early recrystallization near the sediment-water interface is facilitated by the neomorphism of aragonite to calcite (Fig. 7b), allowing for the rapid diffusive and advective supply of seawater calcium. Changes in the rate of sediment accumulation, barring changes in any other processes, would be expected to have a significant impact on the final composition (Fig. 4, top row). The advective flushing of water into sediments, likewise, can provide a source of calcium, changes in the surface advective flux would also be expected to be associated with changes in the final composition (Fig. 4, bottom row). Site 1003 cannot be described using a model with a constant advection rate (Fig. 6), and the best-fitting model shows considerable variance over time, with a significant increase at 12.5 Ma.

4.1. Correlation with changes in platform margin structure

Prior to 13 Ma, calculated vertical fluid advection rates at Site 1003 were lower than those observed after, typically remaining below 2 cm/yr. Around 16 Ma, advection rates appear to have increased to 5 cm/yr, although the calculated uncertainty for this value exceeds the signal itself. Between 13 and 12 Ma, advection rates increase from a prior mean value of 1.9 ± 1.5 cm/yr ($\pm 95\%$ confidence) to the highest calculated rate of 22 ± 14 cm/yr ($\pm 95\%$ confidence) at 12 Ma. This increase in advection correlates with a major re-organization of facies associated with stronger ocean currents in the region (Betzler and Eberli, 2019). This increase in current speed is understood to be a result of tectonic uplift of isthmus of Panama (Haug and Tiedemann, 1998) redirecting currents northward. This change is associated with the onset of drift deposits in the channel, as well as the steepening and progradation of the platform margin. The precise cause for the relationship between fluid advection and the margin and the change in margin structure is murky, and the underlying mechanism is likely the result of many competing forces. It is possible that prior to this transition the advection was affected by the lateral migration of surface fluids, inhibiting the circulation of seawater through the platform margin (Al-Helal et al., 2012; Whitaker et al., 2004). The

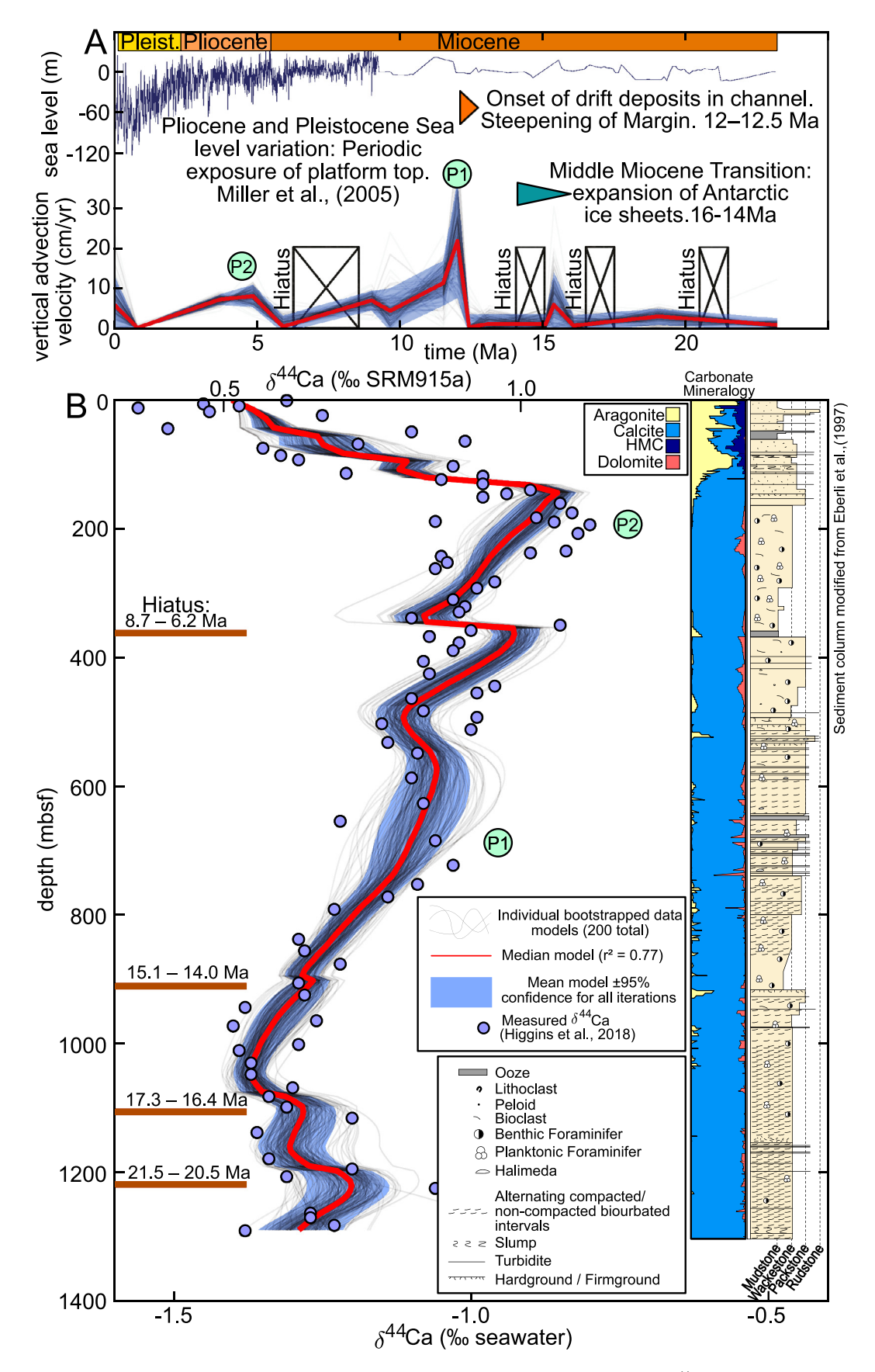


Fig. 7. Calcium isotope advection model for ODP Site 1003. A) Best-fit advection rates for 200 bootstrap resamplings of the δ^{44} Ca data, plotted relative to sediment age. Blue shaded region contains 95% of all models. Red line: median advection rate between all models. Sedimentological and climate events shown according to same timescale. B) Measured (blue circles) and modeled (lines) calcium isotope data for ODP Site 1003 carbonates, shaded region contains 95% of best-fit bootstrap models. Advective Pulses 1 and 2 are labeled as P1 and P2 respectively in both subplots.

observed change could also represent a shift in the location of fluid infiltration, possibly due to the progradation of the platform margin resulting in Site 1003 becoming more platform-proximal. This last explanation does not provide an explanation for the subsequent decrease in fluid infiltration rate after advective pulse 1. Calcium isotope measurements on the more platform-distal Site 1007 also show an increase in $\delta^{44}\mathrm{Ca}$ values although to a lesser degree (Higgins et al., 2018).

The period of diminished advection prior to the Miocene-Pliocene transition occurs partially during a depositional hiatus between 8.7-6.2 Ma, which is accompanied with a relatively minor excursion in measured calcium isotope distributions. If this apparent hiatus were due to the dissolution or re-deposition of the upper sediments, then this interpretation would be false, and a greater magnitude of fluid flow could have been possible at this time. This late Miocene hiatus is also observed at Site 1005 and corresponds to a slowing of deposition at the more platform-distal Sites 1007 and 1006 (Eberli et al., 1997), because of this, it is interpreted as a hiatus rather than being an erosional surface. All other depositional hiatuses occur during the period prior to 13 Ma, wherein modeled advection rates are consistently low. The subsequent increase in advection near the Miocene-Pliocene boundary (Labeled P2 on Fig. 7a), does not coincide with major reorganization sediments in the region.

During the later Pliocene and Pleistocene, advection rates appear to diminish. Changes in ice volume during the Neogene result in significant fluctuations in sea level (Miller et al., 2005), resulting in the platform top being periodically exposed. Although the intensity of ice-volume changes are most extreme during the Pleistocene, changes in Antarctic ice volume likely resulted in sea-level variation during the Miocene as well. Exposure of the platform top is expected to diminish the intensity of Kohout convection on the platform margin (Sanford et al., 1998). It is possible that the frequent exposure of the platform top during the Pliocene and Pleistocene, accompanied with a freshwater lens, resulted in the diminishing advection between Advective Pulse 2 and the present day.

${\it 4.2. Relationship\ between\ advection\ rate\ and\ sediment\ type\ and\ composition}$

There is a notable relationship between the coarsening of sediments above Advective Pulse 1 and the increase in fluid advection rate. Although these coarser sediments may be more permeable to fluid infiltration, as was noted by Caspard et al. (2004), the coarsening of sediments and increase in fluid flow may also be the result of the same forces, namely the increase in benthic current velocity, the steepening of the slope, and the progradation of the platform margin.

Sediments deposited at Site 1003 prior to 15 Ma (910 mbsf) consist of alternating compacted and non-compacted bioturbated wackestone (Fig. 7b; Eberli et al., 1997). Above the hardground surface at 900 mbsf, which corresponds to \sim 1 Ma hiatus of deposition, sediments alternate between coarser-grained packstones and wackestones. This pattern is due to the progradation of the platform margin and variable supply of platform-derived sediments (Eberli et al., 1997).

Dolomite is present in much of the sediment deposited in at Site 1003 (Fig. 7b), although it rarely constitutes the most common mineral phase. The average abundance of dolomite is much higher above Advective Pulse 1 $(3.7\pm0.5\%, 2\sigma)$, than prior $(2.2\pm0.4\%, 2\sigma)$. Advective pulse two is accompanied by particularly high concentrations of dolomite (Fig. 7b), one interpretation of which suggests that the increased supply of seawater (and dissolved magnesium) played a role in promoting dolomitization during this interval. Analyses of dolomite on the platform top (Clino and Unda cores,

measured by Higgins et al. (2018), showed a significant increase in δ^{44} Ca in heavily dolomitized intervals, indicating significant flow of water through the sediments during the dolomitizing process. This interpretation, however, ignores the sulfate reduction and corresponding increase of alkalinity below 100 mbsf at this site (Kramer et al., 2000; Rennie and Turchyn, 2014), which suggests that additional carbonate may have precipitated as a result of these reactions. Recent modeling and analyses conducted by Fantle and Ridgwell (2020) indicate that the magnitude of δ^{44} Ca excursions due to authigenic precipitation is related to the abundance of primary carbonate. Pessimistically, if the 20% dolomite maximum at this depth were formed from unmodified seawater (δ^{44} Ca = 0\%), then this would shift the initial δ^{44} Ca of the sediment package from -1.4% to -1.24 (relative to contemporary seawater), which could account for approximately one third of the observed shift in δ^{44} Ca values at this depth and would bias fluid flow estimates towards more positive values. This worst-case scenario is unlikely for several reasons. If additional carbonate is precipitating at the depth where sulfate is being reduced (>100mbsf) then it is occurring within an essentially closed system with respect to calcium; as Higgins et al. (2018) determined that porefluids below 100 mbsf are at equilibrium with respect to the host carbonate. Additionally, the depletion of sulfate from 30 mM to 20 mM would result in the precipitation of less than 10 mmol of carbonate per liter of porefluid, amounting to an addition of less than 1% carbonate. Nevertheless, the occurrence of dolomite is not unambiguously explained by the model presented in this manuscript, which operates on the assumption that, aside from perturbations in the sediment accumulation rate and changes in the initial isotope ratios, the sediments remain largely similar over time. If sediments deposited during a specific interval were more susceptible to rapid dolomitization, then this would be difficult to account for as it is presently structured. Nevertheless, the increased abundance of in sediments younger than 12.5 Ma seems to indicate that the increased advective supply of seawater magnesium played a role in governing the abundance of this mineral in the platform mar-

There appears to be a broad correlation between sediment type and the magnitude advective flow, although this is most likely due to the common factors affecting both, rather than a specific mechanistic link such as increased permeability. The increase in abundance of dolomite above Advective Pulse 1 indicates more open-system diagenetic reactions occurring due to the increase in advective flow. It is unknown if some this dolomite precipitated purely in a replaceative fashion, however; if a net precipitation of dolomite occurred in shallow sediments, it is possible that it may have biased the advection rate estimates towards slightly more positive values. The change in advective flux clearly affected the isotopic composition of the more rock-buffered elements in the carbonate (e.g. Ca or C), although it does not appear to be the sole predictor for the extent of dolomitization on the platform margin.

5. Conclusions

Analyses of carbonate clumped and calcium isotopes coupled with a reaction-diffusion-advection model informed by the sedimentary history of ODP Site 1003 reveal that there was a change in the intensity of calculated vertical fluid advection rates on the leeward margin of Great Bahama Bank approximately 12–13 Ma. This study demonstrates the utility clumped isotopes to constrain the rate of recrystallization of the sediments, which then enabled the use of calcium isotopes and a Reaction-Diffusion-Advection model to calculate the magnitude of advection in the sediment. A major change in the rate of fluid advection coincided with early stages of the closure of the Isthmus of Panama and the initia-

tion of the Florida Current, a period wherein the leeward margin of the GBB prograded basinward and transitioned from a shallow carbonate ramp to the modern steep rimmed margin. The increase in fluid advection rate at this time may be the result of the sediments becoming more platform proximal, as well as changes in the interaction between the geothermally driven Kohout convection and refluxed surface fluids resulting in an intensification of advection on the platform margin. This advective process is commonly invoked as a mechanism for the ventilation of upper sediments and the transportation of cations (e.g. Mg) into the platform, facilitating the formation of authigenic minerals such as dolomite. Large-scale changes in platform geometry, as well as changes in sediment type correlated with perturbations in the magnitude of the advective flux on the margin of the GBB. These results predict that large-scale changes in sedimentary structure in modern and ancient carbonate systems would be expected to be associated with changes in the open/closed system nature of the diagenetic reactions occur in upper sediments. A number of ambiguities remain in the approach implemented here, a particular limitation being the use of a 1-dimensional model to describe a complex three-dimensional system, future work may benefit from the analysis of additional locations and with the implementation of 2-D and 3-D hydrological models for this system.

CRediT authorship contribution statement

Philip T. Staudigel: Conceptualization, Methodology, Software, Writing and Editing, Data Acquisition, Visualization. **John Higgins:** Data curation, Writing, Data Acquisition. **Peter Swart:** Data Curation, Writing and Editing, Data Acquisition.

Declaration of competing interest

The authors declare no conflicts of interest regarding material related to this publication. All data used in this study are credited to their respective publications.

Acknowledgements

Ian Thomas is thanked for his assistance in operating the AR-CCA Cluster. Two anonymous reviewers provided invaluable insight and resulted in significant refinement and improvement of this manuscript.

Appendix A. Supplementary material

Supplementary material related to this article can be found online at https://doi.org/10.1016/j.epsl.2020.116625.

References

- Ahm, A.S.C., Bjerrum, C.J., Blättler, C.L., Swart, P.K., Higgins, J.A., 2018. Quantifying early marine diagenesis in shallow-water carbonate sediments. Geochim. Cosmochim. Acta 236, 140–159. https://doi.org/10.1016/j.gca.2018.02.042.
- Al-Helal, A.B., Whitaker, F.F., Xiao, Y., 2012. Reactive transport modeling of brine reflux: dolomitization, anhydrite precipitation, and porosity evolution. J. Sediment. Res. 82, 196–215. https://doi.org/10.2110/jsr.2012.14.
- Anselmetti, F.S., Eberli, G.P., Ding, Z.D., 2000. From the Great Bahama Bank into the Straits of Florida: a margin architecture controlled by sea-level fluctuations and ocean current. Bull. Geol. Soc. Am. 112, 829–844. https://doi.org/10.1130/0016-7606(2000)112<829:FTGBBI>2.0.CO;2.
- Baker, P.A., Kastner, M., 1981. Constraints on the formation of sedimentary dolomite. Science 213, 214–216. https://doi.org/10.1126/science.213.4504.214.
- Betzler, C., Eberli, G.P., 2019. Miocene start of modern carbonate platforms. Geology 47, 771–775. https://doi.org/10.1130/G45994.1.
- Betzler, C., Eberli, G.P., Alvarez Zarikian, C.A., Alonso-García, M., Bialik, O.M., Blättler, C.L., Guo, J.A., Haffen, S., Horozal, S., Inoue, M., the Expedition 359 Scientists, 2017. Expedition 359 summary. In: Proceedings of the International Ocean Discovery Program, vol. 359.

- Betzler, C., Reijmer, J.J.G., Bernet, K., Eberli, G.P., Anselmetti, F.S., 1999. Sedimentary patterns and geometries of the Bahamian outer carbonate ramp (Miocene-Lower Pliocene, Great Bahama Bank). Sedimentology 46, 1127–1143. https://doi.org/10.1046/j.1365-3091.1999.00268.x.
- Blättler, C.L., Henderson, G.M., Jenkyns, H.C., 2012. Explaining the Phanerozoic Ca isotope history of seawater. Geology 40, 843–846. https://doi.org/10.1130/G33191.1.
- Boudreau, B.P., 1997. Diagenetic Models and Their Implementation. Springer, Berlin. Burchette, T.P., Wright, V.P., 1992. Carbonate ramp depositional systems. Sediment. Geol. 79, 3–57. https://doi.org/10.1016/0037-0738(92)90003-A.
- Caspard, E., Rudkiewicz, J.L., Eberli, G.P., Brosse, E., Renard, M., 2004. Massive dolomitization of a Messinian reef in the Great Bahama Bank: a numerical modelling evaluation of Kohout geothermal convection. Geofluids 4, 40–60. https://doi.org/10.1111/j.1468-8123.2004.00071.x.
- De La Rocha, C.L., DePaolo, D.J., 2000. Isotopic evidence for variations in the marine calcium cycle over the Cenozoic. Science 289, 1176–1178. https://doi.org/10.1126/science.289.5482.1176.
- Eberli, G.P., Anselmetti, F.S., Kroon, D., Sato, T., Wright, J.D., 2002. The chronostratigraphic significance of seismic reflections along the Bahamas transect. Mar. Geol. 185, 1–17. https://doi.org/10.1016/S0025-3227(01)00287-0.
- Eberli, G.P., Swart, P.K., Malone, M.J., et al., 1997. In: Proceedings of the Ocean Drilling Program, vol. 166, Initial Reports, Bahamas Transect. Ocean Drilling Program
- Fantle, M.S., DePaolo, D.J., 2007. Ca isotopes in carbonate sediment and pore fluid from ODP site 807A: the Ca²⁺_(aq)-calcite equilibrium fractionation factor and calcite recrystallization rates in Pleistocene sediments. Geochim. Cosmochim. Acta 71, 2524–2546. https://doi.org/10.1016/j.gca.2007.03.006.
- Fantle, M.S., Ridgwell, A., 2020. Towards an understanding of the Ca isotopic signal related to ocean acidification and alkalinity overshoots in the rock record. Chem. Geol. 547, 119672. https://doi.org/10.1016/j.chemgeo.2020.119672.
- Farkaš, J., Buhl, D., Blenkinsop, J., Veizer, J., 2007. Evolution of the oceanic calcium cycle during the late Mesozoic: evidence from δ^{44/40}Ca of marine skeletal carbonates. Earth Planet. Sci. Lett. 253, 96–111. https://doi.org/10.1016/j.epsl.2006. 10.015.
- Feary, D.A., Hine, A.C., Malone, M.J., 2000. Leg 182 summary: Great Australian Bight Cenozoic cool-water carbonates. In: Proceedings of the Ocean Drilling Program, Part A: Initial Reports, p. 182.
- Gerya, T., 2010. Introduction to Numerical Geodynamic Modelling, first edition.

 Cambridge University Press.
- Gussone, N., Eisenhauer, A., Heuser, A., Dietzel, M., Bock, B., Böhm, F., Spero, H.J., Lea, D.W., Bijma, J., Nägler, T.F., 2003. Model for kinetic effects on calcium isotope fractionation (δ^{44} Ca) in inorganic aragonite and cultured planktonic foraminifera. Geochim. Cosmochim. Acta 67, 1375–1382. https://doi.org/10.1016/S0016-7037(02)01296-6.
- Haug, G.H., Tiedemann, R., 1998. Effect of the formation of the Isthmus of Panama on Atlantic Ocean thermohaline circulation. Nature 393, 673–676.
- Henderson, G.M., Slowey, N.C., Haddad, G.A., 1999. Fluid flow through carbonate platforms: constraints from ²³⁴U/²³⁸U and Cl⁻ in Bahamas pore-waters. Earth Planet. Sci. Lett. 169, 99–111. https://doi.org/10.1016/S0012-821X(99)00065-5.
- Higgins, J.A., Blättler, C.L., Lundstrom, E.A., Santiago-Ramos, D.P., Akhtar, A.A., Crüger Ahm, A.S., Bialik, O., Holmden, C., Bradbury, H., Murray, S.T., Swart, P.K., 2018. Mineralogy, early marine diagenesis, and the chemistry of shallow-water carbonate sediments. Geochim. Cosmochim. Acta 220, 512–534. https://doi.org/10.1016/j.gca.2017.09.046.
- Kaufman, J., 1994. Numerical models of fluid flow in carbonate platforms: implications for dolomitization. J. Sediment. Res. A Sediment. Petrol. Process. 64A, 128–139. https://doi.org/10.1306/d4267d2f-2b26-11d7-8648000102c1865d.
- Kohout, F.A., 1965. A hypothesis concerning cyclic flow of salt water related to geothermal heating in the Floridan aquifer. Trans. N. Y. Acad. Sci. 28, 249–271.
- Kramer, P.A., Swart, P.K., De Carlo, E.H., Schovsbo, N.H., 2000. Overview of interstitial fluid and sediment geochemistry, sites 1003-1007 (Bahamas transect). Proc. Ocean Drill. Program Sci. Results 166, 179–195. https://doi.org/10.2973/odp.proc.sr.166.117.2000.
- Lemarchand, D., Wasserburg, G.J., Papanastassiou, D.A., 2004. Rate-controlled calcium isotope fractionation in synthetic calcite. Geochim. Cosmochim. Acta 68, 4665–4678. https://doi.org/10.1016/j.gca.2004.05.029.
- Lüdmann, T., Paulat, M., Betzler, C., Möbius, J., Lindhorst, S., Wunsch, M., Eberli, G.P., 2016. Carbonate mounds in the Santaren Channel, Bahamas: a current-dominated periplatform depositional regime. Mar. Geol. 376, 69–85. https://doi.org/10.1016/j.margeo.2016.03.013.
- McCullough, M.L., Land, L.S., 1992a. Dynamic hydrology and diagenesis of a submerged Pleistocene fringing reef, Discovery Bay, Jamaica. Mar. Geol. 104, 139–151.
- McCullough, M.L., Land, L.S., 1992b. Diagenetic history of a submerged Pleistocene Jamaican fringing reef. Carbonat. Evapor. 7, 2–10. https://doi.org/10.1007/BF03175388.
- Miller, K.G., Kominz, M.A., Browning, J.V., Wright, J.D., Mountain, G.S., Katz, M.E., Sugarman, P.J., Cramer, B.S., Christie-Blick, N., Pekar, S.F., 2005. The Phanerozoic record of global sea-level change. Science 310, 1293–1298. https://doi.org/10.1126/science.1116412.

- Nagihara, S., Wang, K., 2000. Geothermal regime of the western margin of the Great Bahama Bank. In: Proceedings of the Ocean Drilling Program, Scientific Results. Ocean Drilling Program, pp. 113–120.
- Rennie, V.C.F., Turchyn, A.V., 2014. The preservation of $\delta^{34}S_{SO4}$ and $\delta^{18}O_{SO4}$ in carbonate-associated sulfate during marine diagenesis: a 25 Myr test case using marine sediments. Earth Planet. Sci. Lett. 395, 13–23. https://doi.org/10.1016/j.epsl.2014.03.025.
- Richter, F.M., DePaolo, D.J., 1987. Numerical models for diagenesis and the Neogene Sr isotopic evolution of seawater from DSDP site 590B. Earth Planet. Sci. Lett. 83, 27–38. https://doi.org/10.1016/0012-821X(87)90048-3.
- Sanford, W.E., Whitaker, F.F., Smart, P.L., Jones, G., 1998. Numerical analysis of seawater circulation in carbonate platforms: I. Geothermal convection. Am. J. Sci. 298, 801–828.
- Schlager, W., Ginsburg, R.N., 1981. Bahama carbonate platforms—the deep and the past. Mar. Geol. 44, 1–24.
- Schmitt, A.D., Bracke, G., Stille, P., Kiefel, B., 2001. The calcium isotope composition of modern seawater determined by thermal ionisation mass spectrometry. Geostand. Newsl. 25, 267–275. https://doi.org/10.1111/j.1751-908x.2001.tb00602.x.
- Simms, M., 1984. Dolomitization by Groundwater-Flow System in Carbonate Platforms.
- Staudigel, Philip T., Murray, S., Dunham, D.P., Frank, T.D., Fielding, C.R., Swart, P.K., 2018a. Cryogenic brines as diagenetic fluids: reconstructing the diagenetic history of the Victoria Land Basin using clumped isotopes. Geochim. Cosmochim. Acta 224, 154–170. https://doi.org/10.1016/j.gca.2018.01.002.

- Staudigel, P.T., Murray, S., Dunham, D.P., Frank, T.D., Fielding, C.R., Swart, P.K., 2018b. Cryogenic brines as diagenetic fluids: reconstructing the diagenetic history of the Victoria Land Basin using clumped isotopes. Geochim. Cosmochim. Acta 224. https://doi.org/10.1016/j.gca.2018.01.002.
- Staudigel, P.T., Swart, P.K., 2019. A diagenetic origin for isotopic variability of sediments deposited on the margin of Great Bahama Bank, insights from clumped isotopes. Geochim. Cosmochim. Acta 258, 97–119. https://doi.org/10.1016/j.gca. 2019.05.002.
- Swart, P.K., 2000. The oxygen isotopic composition of interstitial waters: evidence for fluid flow and recrystallization in the margin of the Great Bahama Bank. Proc. Ocean Drill. Program Sci. Results 166, 91–98. https://doi.org/10.2973/odp. proc.sr.166.130.2000.
- Wang, J., Mooers, C.N.K., 1998. Three-dimensional perspectives of the Florida current: transport, potential vorticity, and related dynamical properties. Dyn. Atmos. Ocean. 27, 135–149. https://doi.org/10.1016/s0377-0265(97)00004-3.
- Whitaker, F.F., Smart, P., Sanford, W.E., States, U., Survey, G., 2004. Numerical Analysis of Seawater Circulation in Carbonate Platforms: II. The Dynamic Interaction Between Geothermal and Brine Reflux Circulation.
- Wright, J.D., Kroon, D., 2000. Planktonic foraminiferal biostratigraphy of leg 166. Proc. Ocean Drill. Program Sci. Results 166, 3–12. https://doi.org/10.2973/odp.proc.sr.166.101.2000.
- Zhang, S., Zhou, R., DePaolo, D.J., 2020. The seawater Sr/Ca ratio in the past 50 Myr from bulk carbonate sediments corrected for diagenesis. Earth Planet. Sci. Lett. 530, 115949. https://doi.org/10.1016/j.epsl.2019.115949.